

DYNAMICS OF A SOLENOID ACTUATED PNEUMATIC SYSTEM

Y. Chait, Research Assistant and C. Radcliffe, Associate Professor
Department of Mechanical Engineering
and
A. H. Case Center for Computer-Aided Design
Michigan State University
East Lansing, Michigan

ABSTRACT

Pneumatic systems controlled by solenoid or servo valves are common parts of industrial control systems. A pneumatic system was developed to apply active vibration control forces. The dynamics of the system was studied through a simulation model and verified through laboratory measurements of a prototype's dynamic response. The simulation model consisted of two coupled subsystems. The electromechanical subsystem models solenoid valve and plunger dynamics. The fluid subsystem models the pressure-flow dynamics through the valve, piping and diffuser. The model results and measurements agreed well and showed that control forces could be generated with amplitudes of 70 Newtons to frequencies up to 30 hz. The model and prototype are in use in the development of an active control system for rotating discs.

T = temperature
t = time
X = displacement
V = volume
v = velocity
 λ = flux linkage
 ρ = density

INTRODUCTION

Pneumatic systems controlled by solenoid or servo valves are common parts of industrial control systems. They are commonly used to control the drive of mechanical actuators, however, the system discussed here uses air pressure forces directly. The system studied (Fig. 1) was designed as a component of a vibration control system for circular saws and other rotating moving plate systems. Previously [1,2], electromagnets have been used to develop control forces which damp plate vibration, however, electromagnets are not practical for applying transverse control forces to some rotating disc systems, e.g. computer disc drives.

NOMENCLATURE

A_d = diffuser cross section area
 A_p = plunger cross section area
 A_v = annular valve discharge area
 A_e = discharge area between diffuser and plate
C = spring compliance
 C_v = valve flow coefficient
E = energy
e = voltage
F = pressure differential force on plunger
f = electromagnet force
I = inertia
i = current
K = discharge flow coefficient
k = specific heat ratio
L = inductance
M = mass
m = mass flow rate
P = pressure
 R_u = universal gas constant
 P_m = momentum
R = electrical resistance
SG = specific gravity

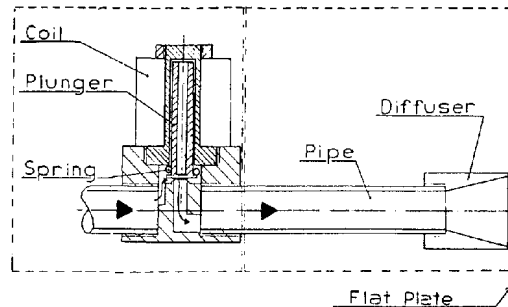


Figure 1: Cross section of the pneumatic force generator system

The pneumatic system was designed to provide a time-varying, controlled force on a flat plate placed across the exit area of the diffuser. The force was developed by pressurization of the diffuser by air flow through a solenoid valve. The system operates in a bang-bang mode: valve closed, or valve open, in response to drive voltages from an external controller. When control forces are applied opposing plate velocities normal to the plate surface, kinetic energy of the plate is removed and plate damping is increased. Acceptable performance of the pneumatic force generator was specified as 22-44 newtons maximum force capability up to a maximum operating frequency of 30 Hz. The purpose of this study was to explore the magnitude of the forces developed on the plate, find the response time of the pneumatic system, and develop a simulation model for use in simulations of circular disc vibration control systems.

The work discussed includes both the development of a simulation model and the laboratory testing of a prototype system. The simulation model was developed from the configuration of the prototype and parameter values assigned by independent measurements of system components. A set of pneumatic system flow and generated force measurements were then made in the laboratory for comparison with simulation results using the above parameters.

PNEUMATIC SYSTEM

The pneumatic system (Fig. 1) consisted of a solenoid valve, short pipe and a diffuser. The pressure at the discharge plane of the diffuser generated a force on the flat plate. A simulation was developed to predict this force using a bond graph [7] model which consisted of lumped parameter elements linked together by a junction structure whose bonds represented power flow. The power variables were force and velocity in the mechanical components, pressure and volume flow rate in the fluid components, as well as voltage and current in the electrical components. The bond graph model provided both a unified method to model the different power types and a systematic technique to extract system state equations. The pneumatic system simulation included two subsystems: an electromechanical subsystem to study the solenoid valve dynamics and a fluid subsystem to study the air flow dynamics.

Electromechanical Subsystem

The bond graph model of a solenoid valve is shown in Fig. 2. The coupling between electrical and mechanical behavior was represented by a mixed IC element which included the coil inductance and the force-displacement relationship (compliance) from the coil's magnetic field on the plunger. The solenoid was a mixed energy storage element where the inductance, L , was a function of the plunger position, X_c , within the magnetic core, while the force on the plunger from the magnetic compliance, C , was a function of the coil flux linkage, λ . Other elements of the model included return spring stiffness, $C3$; plunger mass, $I3$; plunger viscous friction, $R5$; and coil resistance, $R4$. The bond graph also showed the effect of force, F , on the plunger generated by the pressure difference ($P1-P2$, derived below) across the valve plunger cross section, A_p , and the driving voltage, E , across the coil. The bond graph showed the system to have four state variables: X_c and λ as well as return spring deflection, X_s , and plunger momentum, P_m .

The IC element was assumed to be conservative with zero initial stored energy so that the electromechanical energy stored in the IC element was the integral of the mechanical and the electrical power flows into the element.

$$E(\lambda, X_c) = \int_0^t (i \dot{\lambda} + f \dot{X}_c) dt = \int_{0,0}^{\lambda, X_c} (i d\lambda + f dX_c) \quad (1)$$

assuming the IC element has linear electrical characteristics, an inductance, $L(X_c)$ was defined, resulting in the following relationship between λ and the coil current, i .

$$i = \frac{\lambda}{L(X_c)} \quad (2)$$

the conservative IC element had stored energy strictly dependent on the states X_c and λ . Since f vanishes for $i=0$, we set $i=0$ and fixed X_c at its final value doing no work on the element, then evaluated (1) as

$$E(\lambda, X_c) = \int_0^\lambda i d\lambda = \frac{\lambda^2}{2 * L(X_c)} \quad (3)$$

The force produced by the magnetic field was derived from (1) using (3)

$$f = \frac{\partial E}{\partial X_c} = \frac{\lambda^2}{2 * L^2(X_c)} * \frac{d}{dX_c} L(X_c) \quad (4)$$

The state equation for the coil flux linkage was extracted from Fig. 3 by summing the voltages on the coil current which included the drive voltage and the voltage dissipation across the coil resistance.

$$\frac{d\lambda}{dt} = e - i * R4 \quad (5)$$

The state equation for the plunger momentum was extracted from Fig. 2 by summing the forces on the plunger velocity which included the magnetic force, spring and damping forces and the force introduced by

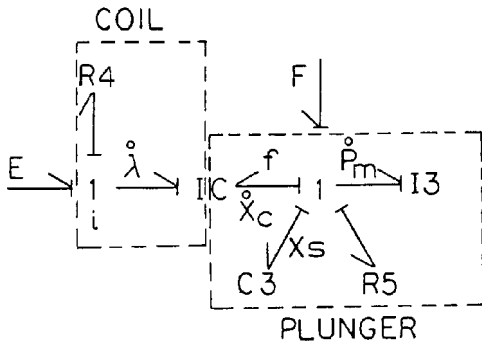


Figure 2: Bond graph model of the electromechanical subsystem

the pressure difference across the valve, F.

$$\frac{dP_m}{dt} = -f - \frac{X_s}{C} - R5 * \frac{P_m}{M} - F \quad (6)$$

The state equations for plunger and spring displacements were

$$\frac{dX_s}{dt} = \frac{P_m}{M} \quad (7)$$

$$\frac{dX_c}{dt} = \frac{P_m}{M} \quad (8)$$

These state variables had identical state equations however, their initial conditions were independent.

Fluid Subsystem

The bond graph model of the fluid subsystem (Fig. 3) included system parameters: pipe-diffuser air compliance, C1; the solenoid valve flow resistance, R2; and the diffuser discharge plane flow resistance, R3. The bond graph model was driven by air pressure applied at the valve inlet, P1, and the atmospheric air pressure at the diffuser exit plane, Pa. The bond graph showed the subsystem to have one state variable. In this case, pipe-diffuser pressure, P2, was used.

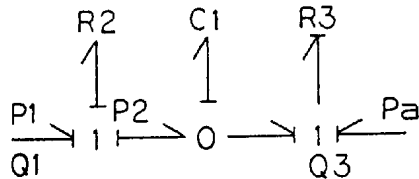


Figure 3: Bond graph model of the fluid subsystem

The total force applied on the plate was derived from integration of static pressure. A diffuser recovers potential energy (static pressure) from kinetic energy (flow velocity). However, increasing the diffuser angle eventually results in a stall, and negative pressure on the disc face. Kline's [12] work on optimum design of straight-walled diffusers provides us with the proper dimensions for maximum pressure recovery. We used a 10 deg. expansion angle in the design discussed here. Several expressions [13,14] for the total force on the disc exist, however, in the absence of significant stall regions, the pressure distribution on the plate was assumed uniform, and

$$FORCE = \int_0^{A_d} P2 * dA = P2 * A_d \quad (9)$$

where the effective area, A_d, is the diffuser exit area.

From the equation of state for a perfect gas, it can be shown that

$$\frac{dP2}{dt} = (m_2 - m_1) * \frac{R_g * T}{V} \quad (10)$$

where the mass flow rates, m₂ and m₁, were functions of the flow resistance R2 and R3 to be derived below.

Two flow regions were defined in the subsystem: free and choked. Choked flow occurred when the pressure ratio across an element exceeded the critical ratio of 1.89 [9]. At free flow conditions, m₂ was the product of Q1 and the inlet air density and the expression used (Equ. 11) for the volume flow rate across a solenoid valve was that proposed by The National Fluid Power Association [10].

$$Q1 = 22.48 * Cv * \frac{P1 - P2}{T * SG} \quad (11)$$

A similar relationship was used for the discharge volume flow rate, Q3, as a function of (P2 - Pa).

$$Q3 = K * A * \frac{(P2,3 - Patm)}{\rho} \quad (12)$$

and by assuming an isentropic model for a real adiabatic process we used the pressure-density relationship,

$$P * \rho^{1/k} = \text{constant}. \quad (13)$$

although there was a temperature increase for the isentropic process, we assumed that it was negligible. For example, a 5 degree change from an average temperature of 20 degree centigrade results in less than one percent error in density calculations.

For pressure ratios above 1.89 an increase in the pressure, P1, resulted in a proportional increase in m₂ with no change in Q1, while changes in P2 had no effect [9]. Mass flow rate, m₁, was calculated from [11]

$$m_2 = 0.532 * Cv * A_v * P1 * \frac{1}{T} \quad (14)$$

and mass flow rate m₁ was calculated as the product of choked Q3 with ρ obtained from (13) for P = P3.

Flow coefficients, Cv and K, were determined empirically (Fig. 7-8). For the solenoid valve, Cv was assumed to be linearly related to plunger displacement [8].

EXPERIMENTAL RESULTS

A laboratory teststand was constructed to validate the simulation model, evaluate the force on the plate, and the required air flow rate. The prototype pneumatic system on the teststand (Fig. 4a) consisted of a KIP, Inc. solenoid valve with 0.25 inch orifice (model 6X206) mounted on a 9.525 mm (3/8 in.) pipe. The standard solenoid return spring with 300 N/m stiffness was replaced by a spring with a stiffness of 4000 N/m and initial compression of 12.7 mm with the valve closed. This spring was installed to decrease valve closing time. The

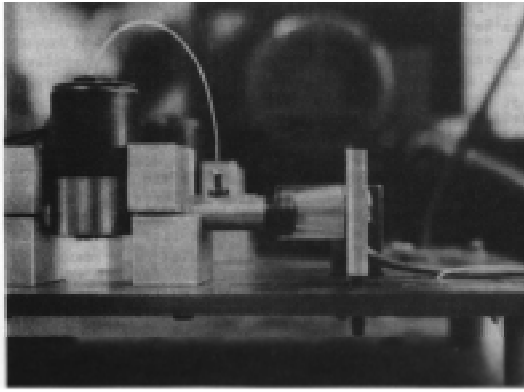


Figure 4a: Laboratory test system showing the solenoid valve, pipe, diffuser and plate. Note pressure tap installed on pipe.

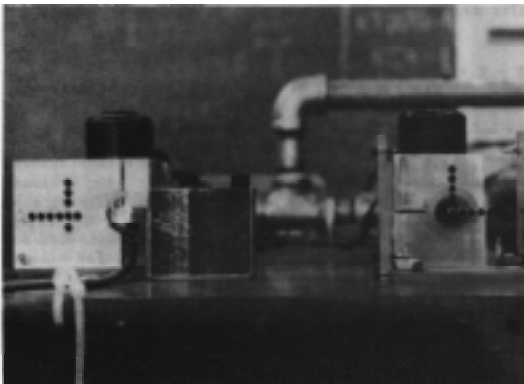


Figure 4b: The pair of plates used to test force generated. The transparent right-hand plate shows the location of pressure taps relative to the diffuser. The left-hand plate is the strain gage load cell used.

diffuser was mounted downstream of the valve on a 76.2 mm long, 9.525 mm (3/8 in.) pipe section. The diffuser was fabricated from 25.4 mm O.D. plexiglas with its O.D. expanding from 12.7 mm to approximately 19 mm (10 deg. expansion angle) over its 19 mm length. The diffuser expansion yielded a 37 percent increase in cross sectional area over the pipe cross section.

Total air volume flow rate through the system was measured with a standard ASME flow meter, consisting of a 50.8 mm (2 inch) pipe thin-plate orifice mounted between flanges [16-18]. The force on the plate was measured with a force transducer (Fig. 4b) fabricated from four active strain gages in Wheatstone bridge configuration [18]. Pressure distribution on the plate, as well as pressures downstream and upstream of the solenoid valve were measured with Entran Devices, Inc. (model no. EP15-80CK-100) pressure transducers. Dynamic pressure and force data was collected with a PDP-11/02 minicomputer and 12 bit analog-to-digital

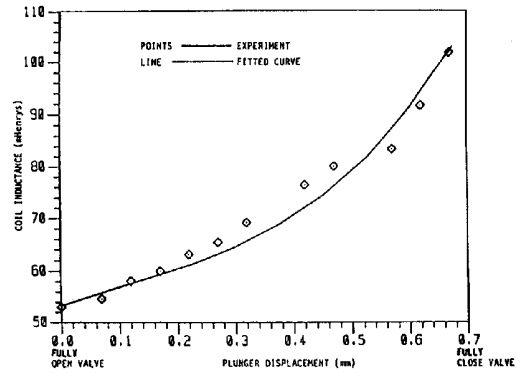


Figure 5: Coil inductance vs. plunger displacement

converter with a 10,000 Hz. sampling rate. Equations (10) to (14) were used to convert pressure differences across the solenoid valve to volume flow rates. The measured coil inductance is shown in Fig. 5. Flow coefficients for the valve (Fig. 6) and the discharge plane (Fig. 7) were found by calibration with the flow meter [18] in accordance with ASME specifications [16,17].

Two flow regions were observed during operation of the pneumatic system. The steady state force behavior was found to be nearly linear in each regime (Fig. 8). For an inlet pressure of 544 KPa (all pressures are absolute) and diffuser-plate gaps above 0.45 mm., a plate force sensitivity of approximately 12.26 N/mm was observed. Below a gap of 0.45 mm., a sensitivity of approximately 175 N/mm was observed. Also shown, are steady state force and volume flow rate results from the simulation model indicated by solid lines. As expected, there was good correlation between the steady-state measurements and steady-state simulation results because of the empirically determined discharge coefficients. At gaps less than 0.25 mm., the variation between measured and calculated forces increased due to reattachment of the separated flow at the diffuser lip which resulted (Fig. 9) in a negative pressure region on the diffuser periphery not included in the simulation model. This negative pressure phenomena is typical for devices with geometry such as nozzle-flapper devices [15].

For gaps above 0.45 mm and 544 KPa inlet pressure, choked flow occurred across the valve and free flow occurred across the diffuser because diffuser pressure was below 192 Kpa. In this region, the valve limited the air flow rate and flow rate was unaffected by the diffuser gap (Fig. 8).

For gaps below 0.45 mm and 544 Kpa inlet pressure, the diffuser pressure was increased above the critical 192 Kpa level and choked diffuser exit flow occurred. At gaps between 0.18 and 0.45 mm, both flows were choked, i.e. diffuser pressure between 192 KPa and 290 KPa. Below 0.18 mm diffuser gap, the diffuser pressure was above 290 KPa and free flow occurred across the valve. In this region, the flow is controlled by the diffuser gap, nearly independent of the valve flow (Fig. 8).

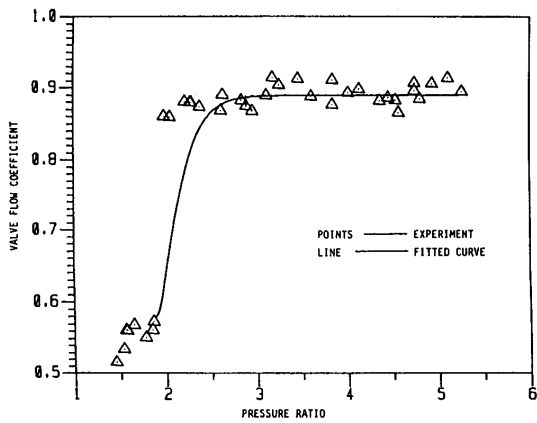


Figure 6: Flow coefficient for the solenoid valve

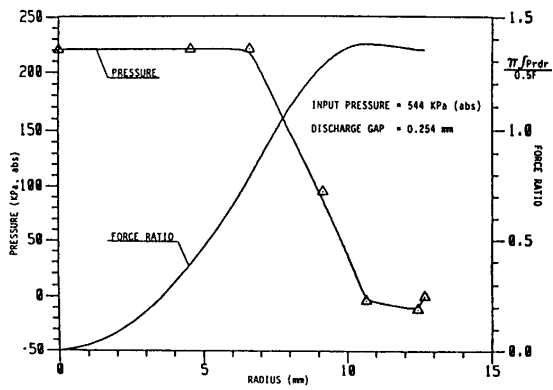


Figure 9: Measured Pressure distribution on the plate

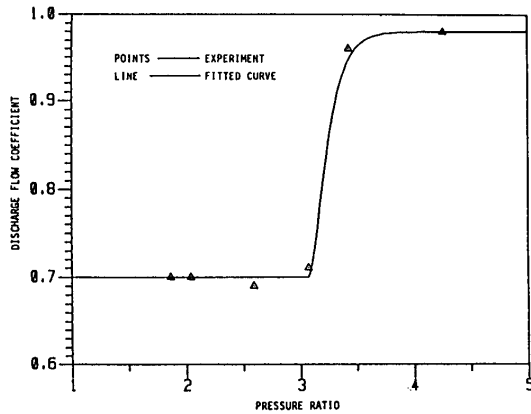


Figure 7: Flow coefficient for the diffuser

Step responses of the laboratory prototype at three diffuser gaps for 544 Kpa inlet pressure were compared with simulation results (Fig. 10) to evaluate the accuracy of the simulation. Measured forces are shown along with forces calculated from the diffuser pressure predicted by the simulation. The second order or higher dynamics of the measured response agreed well with the fourth order, nonlinear simulation model. The simulation predicted a shorter opening time for the valve than measured. The 1.5-2.0 msec difference probably resulted from not including eddy current effects in the simulation model. Eddy current reduces the rate of coil flux build up and thus increase the valve opening time as observed in Fig. 10.

The pressure increased towards steady state at comparable rates in both measured and predicted responses. This observation confirmed the modelling accuracy of the fluid compliance element. The measured responses included high frequency oscillations at approximately 600 Hz. This frequency

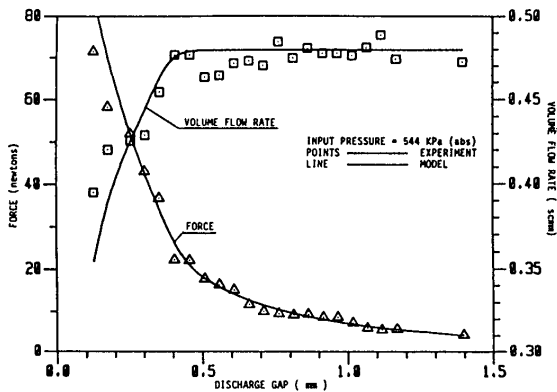


Figure 8: Force on plate and diffuser volume flow rate versus plate-diffuser discharge gap

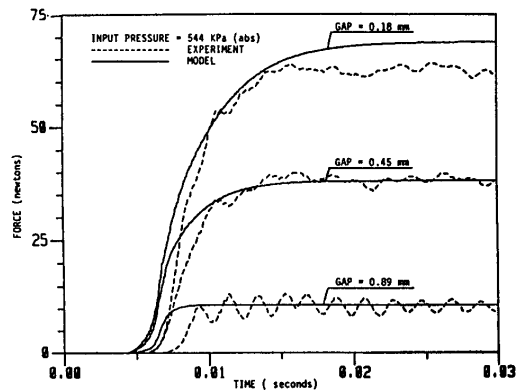


Figure 10: Pneumatic system step input response

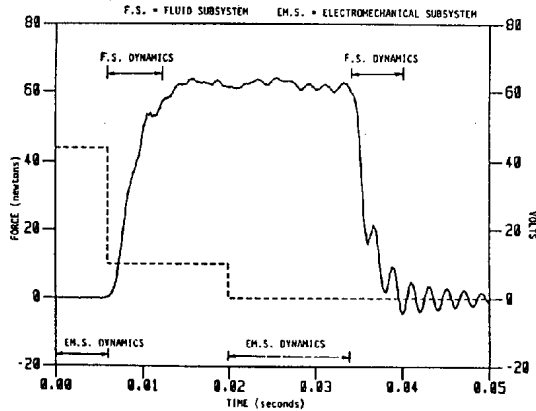


Figure 11: Measured pneumatic system on-off cycle response

is very close to measured bending and torsional natural frequencies of the force transducer [18]. The sensitivity of the transducer to deflections indicated that the oscillations were less than 0.009 mm and their effect on diffuser gap was negligible.

The measured dynamics of the fluid (F.S.) and electromechanical (E.M.S.) subsystems during an on-off cycle are shown in Figure 11. The total on-cycle force transient consisted of distinct periods associated with separate E.M.S. and F.S. dynamics. The on-cycle began with the application of a 44 Vdc excitation for a time of 6 msec, referred to as the E.M.S. dynamics period, which is the time required for the coil flux to increase to a level where the plunger began to move. At that time, the excitation voltage was reduced to a level required to hold the valve open, decreasing the input power. It then took 6 msec for the F.S. to reach steady state. The off-cycle began with the removal of excitation voltage. The 14 msec E.M.S. transient period observed was the time required for the coil flux to decay to a value where the plunger began to close. The F.S. then required 6 msec for the pressure generated force to decay to zero. These results showed that the minimum force pulse width which could be achieved was 26 msec. Using opposing force generators to achieve bipolar forces then allows control force periods down to 52 msec (19.2 Hz) without overlap. However, using some force overlap, control force frequencies were generated up to 30 Hz.

CONCLUSIONS

The dynamics of a solenoid actuated pneumatic system have been presented. The system was designed for control applications and a simulation model was developed. Laboratory tests were used to independently identify the parameters of the model and the simulation was used to predict steady state and transient responses over a range of diffuser gaps. Laboratory measurements of the static air flow rates and forces generated in the prototype system compared well to predicted values. The differences in the transient response are a result of eddy current effects which currently are not modeled. Eddy current effect can be modeled in a magnetic system coupled with electrical system and should yield better transient results.

The work here provides a basis for evaluating both future design of the same geometry for both electromechanical and fluid components. In the future, diffuser development to reduce air flow rates at the same force levels would improve control efficiency. By applying a reverse voltage on the coil during the off-time the closing time could be reduced, improving system frequency response. The system as designed meets the original design force specification. The system is currently under evaluation in a laboratory prototype circular disc control system.

ACKNOWLEDGEMENT

The authors gratefully acknowledge the support of this research by the National Science Foundation through grant MEA 82 05008.

REFERENCES

1. Radcliffe, C. J., and Mote, C. D., Jr., "Identification and Control of Rotating Disc Vibration", ASME Journal of Dynamic Systems, Measurement, and Control, Vol. 105, March 1983, pp. 39-45.
2. Ellis, R. W., and Mote, C. D., Jr., "A Feedback Vibration Controller for Circular Saws", ASME Journal of Dynamic Systems, Measurement, and Control, Vol. 101, March 1979, pp. 44-49.
3. Karnopp, D., and Rosenberg, R., System Dynamics: A Unified Approach, John Wiley and Sons, 1975.
4. Kline, S. J., Abbott, D. E., and Fox, R. W., "Optimum Design of Straight Walled Diffusers", ASME Journal of Basic Engineering, Sept. 1959, pp. 321-331.
5. Dmitriyev, V. N., and Shashkov, A. G., "Force of the Jet Action on the Baffle in Pneumatic and Hydraulic Control Units", Pneumatic and Hydraulic Control Systems, Vol 1, Pregamon press, 1968, pp. 272-284.
6. Blackburn, J. F., Reethof, G., and Shearer, J. L., Fluid Power Control, The Technology Press of M.I.T., 1960, pp. 313-318.
7. Potter, M. C., and Foss, J. F., Fluid Mechanics, Great Lakes Press Inc., 1982.
8. Fleischer, H., Practical Air Valve Sizing, Numatics Inc., 1973, pp. 9.
9. Shapiro, A. H., The Dynamics and Thermodynamics of Compressible Fluid Flow, The Ronald Press Co., 1953, Vol I, pp. 82-100.
10. Beard, C. S., Final Control Elements: Valves and Actuators, Chilton Co., 1969, pp. 6-9.
11. Chait, Y., Active Control of Mechanical Vibration Utilizing Pneumatic Forces, M.S. Thesis, Dept. of Mech. Engineering, Michigan State University, E. Lansing, MI, Sept. 1984.
12. Bean, H. S., "Fluid Meters, Their Theory and Application", ASME Research Committee on Fluid Meters, 6th edition, 1971.
13. Miller, R. W., Flow Measurement Engineering Handbook, McGraw-Hill, 1983, chap. 8.
14. Wark, C. E., and Foss, J. F., "Forced Caused by the Radial Out-Flow Between Parallel Discs", ASME Journal of Fluids Engineering, Sept. 1984, pp. 292-297.